A Hybrid Localization Algorithm for Wearable Safety Devices

Orlando Tovar Ordoñez
tovarordonez@ismb.it

Francesco Sottile
sottile@ismb.it

Emil Kallias
kallias@ismb.it

Claudio Pastrone
pastrone@ismb.it

Istituto Superiore Mario Boella, PerT Research Area
10138 Via P. C. Boggio, 61
Turin, Italy

ABSTRACT

Occupational safety and health (OSH) in industrial environments is gathering increasing attention in the era of Industry 4.0. In this context, location based services (LBS) can be adopted to support workers' safety in hazardous industrial environments. However, the provision of accurate location service in these harsh environments still faces big challenges.

To address these challenges, this paper presents a robust hybrid localization algorithm that combines ultra-wideband (UWB) based ranging measurements and inertial measurement unit (IMU) data. The algorithm has been implemented on a proprietary wearable platform and its performance has been evaluated in an indoor environment. The experimental results show that the proposed hybrid algorithm outperforms a non-hybrid, UWB-based, $Position - Velocity$ (PV) extended Kalman filter (EKF), which has been chosen as benchmark, in terms of both location accuracy and availability. Thanks to a modular approach, the proposed solution also leads to a lower computation processing compared to other hybrid solutions.

Keywords

Radio-based localization, UWB, IMU, wearable technology, Kalman filter, Industry 4.0.

1. INTRODUCTION

In the era of Industry 4.0 [12], the application of cyber physical systems (CPS) and, in general, the adoption of information and communication technology (ICT) are playing an important role as these contribute to the transformation of traditional working environments in a way that are both more productive and appealing for workers.

Another important aspect of Industry 4.0 is the workplace safety that has been triggering the adoption of innovative ICT solutions mainly based on wearable devices. For example, wearable technology can be used by workers in order to prevent their access to dangerous areas, such as regions of the shop floor in which there is a presence of high heat or toxic gas or other types of hazards. To this purpose, radio frequency (RF) positioning systems can be employed in order to alert workers approaching these dangerous areas. It is remarked that global navigation satellite systems (GNSS) cannot be used for these applications as the satellite signal is obstructed in indoor environments.

Many proposed indoor positioning systems are based on the ultra-wideband (UWB) radio technology as it provides accurate ranging measurements with a precision proportional to the signal bandwidth and independent from the environment [5]. In addition, the UWB technology is low cost, provides lower power consumption, in comparison to other radio technologies, and it is robust against interference and fading. Typically, in office scenarios, the UWB positioning error is in the order of centimetres. However, the performance of UWB-based localization systems is heavily affected in industrial environments due to high amount of metal surfaces, electrical motors, soldering robots, etc. [11]. In order to be more robust, location systems based only on inertial measurement unit (IMU) have been proposed [3][8]. The related position accuracy depends on the sensor quality and the ability to estimate its orientation in a robust way [2]. In addition, these location systems are infrastructure independent as they do not need the deployment of *anchor* nodes and provide good short-term accuracy, but lack in long-term stability due to biased measurements [6].

This paper, presents a hybrid localization system for industrial environments combining UWB-based ranging measurements and IMU data. In particular, the localization system uses a two-cascade Bayesian algorithm for a robust position estimation taking into account drifting problem of IMU sensors. In addition, the localization algorithm estimates the sensors's orientation (named *attitude*) and detect/remove ranging measurements outliers.

This paper is structured as follows: section 2 presents the related works. Section 3 presents the overview of the hybrid localization system as well as the application scenario. Section 4 shows a designed UWB-based wearable device for the hybrid algorithm implementation. Section 5 describes the designed hybrid localization algorithm. Section 6 exposes the experimental results and section 7 concludes this work.

DOI: 10.1145/1235

BODYNETS 2016, December 15-16, Turin, Italy

DOI 10.4108/eai.15-12-2016.2267783

2. RELATED WORKS

Some localization approaches have been proposed in the literature with the aim to enhance their performance in harsh industrial environments. The authors in [9] presented a method to reduce the self-interference of radio-based ranging measurements in order to enhance the accuracy of the estimated position. Other authors have focussed on inertial navigation systems proposing pedestrian dead reckoning localization [3][8]. In order to estimate sensor's orientation in a robust way, mechanisms for bias estimation and *attitude* error compensation have been developed; either by taking assumptions on the movement of persons or introducing additional sensors [6] such as a magnetometer for the heading computation. However, the magnetic field might be highly disturbed in industrial environments making the bias and *attitude* error correction challenging. The authors in [10] presented an effective and adaptive IMU/Magnetometer based filter for an *attitude* and heading reference system (AHRS). The experiments in [10] proved that the proposed method can improve the orientation estimation performance of low-cost IMU sensors. Also the authors in [2] presented a comparison of several state-of-the-art AHRS algorithms proposing an approach to improve their behaviour in industrial environments. Special emphasis has been given to the effects of magnetic perturbations. The experimental results showed that the proposed approach is highly recommended for a better orientation estimation performance in challenging environments.

Furthermore, many authors have proposed hybrid solutions combining different technologies. In [6] a localization system was presented fusing both received signal strength (RSS) ranging measurements and IMU measurements. The system was tested in an industrial environment providing an accuracy of 2 meters [6]. Notwithstanding RSS/IMU fusions are widely used, the localization accuracy is low. UWB/IMU fusions have recently received more attention, since they can achieve good position accuracy even at low update rates of ranging measurements, *e.g.* 1 Hz [4]. The authors in [4] presented a low-cost system for accurate localization in challenging environments that fuses UWB/IMU measurements. The system was tested both in outdoor and indoor environments. It was shown that the hybrid system can maintain a sub-meter accuracy of localization with an UWB update rate reduced from 10 Hz to 0.2 Hz.

The contribution of this paper is a hybrid localization algorithm that has been designed adopting a modular approach. In particular, the algorithm distributes the processing effort in a two-cascade extended Kalman filter (EKF). The first EKF implements the AHRS presented in [10] for the *attitude* estimation. In addition, here the approaches described in [2] are used to improve the performance of the AHRS in industrial environments. The second EKF implements a proposed $Position-Velocity-Acceleration$ (PVA) model to perform the localization. As a result, it is possible to perform reliable pedestrian localization in industrial environments by means of wearable devices and thus support the workers' safety.

3. OVERVIEW OF THE HYBRID LOCALIZATION SYSTEM

Figure 1 presents the overall architecture of the localization system. It consists of an UWB-based indoor positioning system, able to estimate the location of workers on the basis of a prototype UWB-based wearable device. The system is composed of the UWB-based wearable device, presented in more detail in section 4, (named *tag*), UWB fixed nodes (named *anchors*), and an UWB gateway (GW). The *tag* periodically communicates with the *anchors* performing time-of-arrival (ToA)-based ranging measurements [5]. These measurements along with the position of the *anchors* and the inertial measurements collected from the *tag*'s IMU, are processed by the localization algorithm implemented in the wearable device to estimate the worker's position. As soon as the estimated position is available, the *tag* sends it to the GW interacting with a computer which collects the estimated data. Figure 1 shows an example of application scenario related to occupational safety. In this scenario, in order to guarantee the safety, the PC implements an application that provides alerts based on a geo-fencing logics service by using a classical point-in-polygon algorithm: given a set of predefined forbidden/dangerous areas at the shop floor and the estimated workers' position, the geo-fencing application detects wether they are inside these areas, and generates an alarm if necessary.

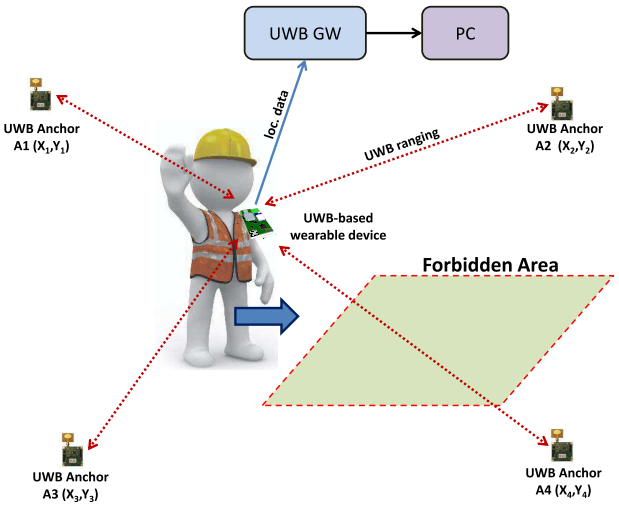

Figure 1: Overall architecture of the localization system.

4. OVERVIEW OF THE UWB-BASED WEARABLE DEVICE

This section presents the hardware (HW) features of the UWB-based wearable prototype, showed Figure 2, that has been used as a *tag* to test the localization algorithm. The size of the prototype is 46 mm x 29 mm.

The STM32F411 ARM Cortex F4 Microprocessor from ST Microelectronics[1] has been selected as the main processing unit. The wearable integrates two different wireless technologies that can be used for communication: a UWB radio module, which is mainly used for localization and small payload communication; and a Bluetooth Low Energy (BLE) module that can be used to transmit information to smartphones and other devices, *e.g.* tablets. In addition, an IMU sensor has been integrated to enable the hybrid localization.

[1]http://www.st.com

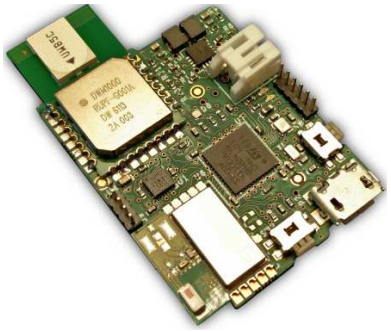

Figure 2: UWB-based wearable platform.

The UWB radio module is based on the DWM1000[2] component which is compliant with the IEEE802.15.4a standard [7]. It allows distance measurements between two devices with an accuracy of up to 10 cm in LoS. Under ideal circumstances this chip will be able to measure distances up to 300 m. The module uses centre frequencies of 3495.4, 3993.6, 4492.8 or 6489.6 MHz respectively and operates at bandwidths of 499.2 or 900 MHz. In addition, the ranging can be performed at data rates of 110 kbps, 850 kbps or 6.8 Mbps.

The BLE module is based on the SPBTLE-RF[3] component which is compliant with the second generation BlueNRG-MS chip[4] and provides a low power solution. This module operates as a radio receiver that also implements most of the Bluetooth 4.1 stack.

Finally, the IMU sensor is based on the MPU9250[5] device which includes a 3-axis gyroscope, 3-axis accelerometer and 3-axis magnetometer in one package.

Furthermore, the prototype also incorporates a USB port, LEDs and free GPIO pins and provides means for adding additional sensors in the future.

5. HYBRID LOCALIZATION ALGORITHM

Figure 3 presents the architecture of the localization algorithm. In particular, there are two main blocks involved in the localization: *Attitude estimator*, presented in section 5.1, and *Location estimator*, presented in section 5.2. The *Attitude estimator* provides orientation information as well as bias tracking for the gyroscope measurements. The *Location estimator* tracks the position and velocity of the target, and the bias of the accelerometer taking as input both the *attitude* and UWB-based range measurements. Since the readings of the sensors (*i.e.* UWB/Inertial/Magnetic measurements) have different update rates, the *attitude* and the localization modules can be executed at different intervals of time; thus, this helps distributing the processing efforts. Moreover, the disturbances that affect the performance of the hybrid algorithm are managed by the *Correction control* block and the outliers filter. The *Correction control* block performs analysis of the IMU measurements. This block is described in section 5.1. The outliers filter processes the ranging measurements and rejects ranging distances. In particular, ranging measurement with respect to an *anchor* can be rejected when the difference between the current estimated distance and the previous one, divided by the time step, is larger than the defined maximum walking speed of a person.

[2]http://www.decawave.com/products/dwm1000-module
[3]http://www.st.com/en/wireless-connectivity/spbtle-rf.html
[4]http://www.st.com/en/wireless-connectivity/bluenrg.html
[5]https://www.invensense.com/products/motion-tracking/9-axis/mpu-9250/

5.1 Attitude estimator

This block uses routines to compute and correct the sensor's *attitude* and the bias of gyroscope measurements by means of: the *Orientation computation*, the *EKF attitude error estimator* and the *Attitude correction* components inside the AHRS block.

The *Orientation computation* uses gyroscope measurements to update the *tag*'s *attitude* by using a Padè approximation [4]. The *attitude* is expressed as the direction-cosine-matrix (DCM) from body (b)-frame to navigation (n)-frame. Since the drift in gyroscope measurements increase in time, an error into the updated *attitude* will increases each time the Padè approximation is performed. Thus a method for tracking the bias and the *attitude* error has to be adopted. To this aim, the AHRS algorithm presented in [10] has been adopted and implemented by the *EKF attitude error estimator* component. This EKF estimates the *attitude* error expressed in Euler angles and the bias of the gyroscope measurements by means of accelerometer/magnetometer measurements in b-frame. The main characteristic of this component is the effective adaptability to set the EKF parameters according to the dynamic scale sensed by the accelerometers. The *Attitude correction* component adjusts the updated *attitude* by means of the tracked errors as in [8].

In general, AHRS algorithms are only able to track the previously mentioned errors in a reliable way under ideal conditions, *i.e.* no significant acceleration and magnetic disturbances. Thus the submodules in the *Correction control* block (*i.e.* SP/ZA/MD detectors) [3] have been fostered to detect the right time to track those errors. Then, the proper time to enable the AHRS block is when no magnetic disturbances are presented (established by the magnetic disturbances (MD) detector), and when there are static periods or zero acceleration instants (determinated by the static periods (SP) detector and the zero acceleration(ZA) detector, respectively).

5.2 Location estimator

This block implements an EKF that uses a PVA model to represent the dynamics of the system. The location of the worker is computed here in two steps: the EKF *predict phase* and the EKF *update phase*. The *predict phase* uses the estimated *attitude* presented in section 5.1, the accelerometer measurements and the dynamic equations to provide the *a priori* location information. The *update phase* uses the UWB-based ranging measurements to update and correct the predicted position by the previous phase as well as to track the bias of the accelerometer. In case the *anchor* connectivity is limited, the *update phase* cannot be implemented. However, *a priori* location information estimated in the *predict phase* can be used to provide accurate position estimation but over a short-period of time. This short-period depends on the bias of the accelerometer readings, since this affects the performance of the predicted positions.

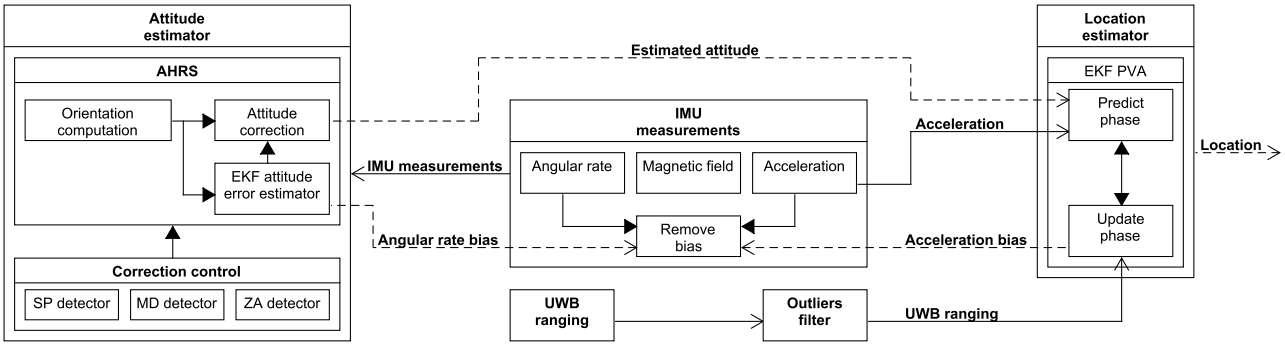

Figure 3: Block Scheme of the Hybrid Localization Algorithm.

5.2.1 EKF PVA Implementation

The EKF performance depends heavily on how well the systems dynamics and measurements, including their statistical characterization, are modelled; therefore, a properly definition of the state model that describes the system dynamics is relevant. This section focuses on the design and development of a low-complexity tracking algorithm in a low dynamics scenario, *i.e.*, localization workers in industrial environments. As mentioned, the dynamics of the system follow a PVA model. The state vector ($\boldsymbol{x}$) in Eq. 1 expresses the position, velocity and acceleration bias expressed in NED (North-East-Down) coordinates.

$$\boldsymbol{x} = [\boldsymbol{p}, \boldsymbol{v}, \delta\boldsymbol{a}]^T, \tag{1}$$

where, $\boldsymbol{p}$ and $\boldsymbol{v}$ are position and velocity vectors, respectively, expressed as $\boldsymbol{p} = [p_n, p_e, p_d]$ and $\boldsymbol{v} = [v_n, v_e, v_d]$, and $\delta\boldsymbol{a}$ is the acceleration bias defined as $\delta\boldsymbol{a} = [\delta a_n, \delta a_e, \delta a_d]$. Where the bias $\delta\boldsymbol{a}$ is the difference between the measured acceleration ($\tilde{\boldsymbol{a}}^n$) and the true acceleration ($\boldsymbol{a}^n$) both in the n-frame as $\delta\boldsymbol{a}^n = \tilde{\boldsymbol{a}}^n - \boldsymbol{a}^n$. In addition, $\tilde{\boldsymbol{a}}^n$ is computed by rotating the accelerometer measurements from b-frame to n-frame by means of the DCM obtained from the *Attitude estimator* (see section 5.1) as $\tilde{\boldsymbol{a}}^n = C_b^n \times \tilde{\boldsymbol{a}}^b$. Where C_b^n is the DCM from b-frame to n-frame.

The equations that describe the dynamics of the system are the following:

$$\boldsymbol{p}_k^n = \boldsymbol{p}_{k-1}^n + \boldsymbol{v}_{k-1}^n \Delta t_k + \boldsymbol{a}_k^n \Delta t_k^2/2, \tag{2}$$

$$\boldsymbol{v}_k^n = \boldsymbol{v}_{k-1}^n + \boldsymbol{a}_k^n \Delta t_k, \tag{3}$$

$$\boldsymbol{a}_k^n = \boldsymbol{a}_k^n, \tag{4}$$

where, Δt_k is the time elapsed between the previous estimation time t_{k-1} and the current estimation time t_k. The measured acceleration in n-frame is considered as an input to the system.

The *predict phase* and the *update phase* are further described in the following.

Predict phase

The discrete EKF state of a dynamic system is modelled by the following discrete time state equation [1].

$$\begin{aligned} \boldsymbol{x}_k &= f(\boldsymbol{x}_{k-1}, \boldsymbol{\mu}_k) + \boldsymbol{w}_k, \\ \boldsymbol{w}_k &\sim \mathcal{N}(\boldsymbol{0}, Q_k), \end{aligned} \tag{5}$$

where $\boldsymbol{x}_k$ is the state vector at time k, f is the state transition function which evolves the previous *a posteriori* state vector $\boldsymbol{x}_{k-1}$ and the input $\boldsymbol{\mu}_k$ to the system. The random process noise vector $\boldsymbol{w}_k$ is modelled as an independent random variable with zero mean and covariance matrix Q_k. The process noise vector takes into account the non-linearity and perturbations of the system.

The prediction of the state vector is estimated as follows:

$$\hat{\boldsymbol{x}}_{k|k-1} = f(\hat{\boldsymbol{x}}_{k-1|k-1}, \boldsymbol{\mu}_k) = F_k \hat{\boldsymbol{x}}_{k-1|k-1} + B_k \boldsymbol{\mu}_k, \tag{6}$$

where $F_k = \frac{\delta f}{\delta x}|_{\hat{\boldsymbol{x}}_{k-1|k-1}}$ is the Jacobian matrix of the state transition function f and B_k relates the input $\boldsymbol{\mu}_k$ with the dynamics of the system.

$$F_k = \begin{bmatrix} I_3 & \Delta t_k I_3 & -C_{bk}^n \Delta t_k^2 I_3/2 \\ 0_3 & I_3 & -C_{bk}^n \Delta t_k I_3 \\ 0_3 & 0_3 & I_3 \end{bmatrix}, \tag{7}$$

$$B_k = \begin{bmatrix} \Delta t_k^2 I_3/2 \\ \Delta t_k I_3 \\ 0_3 \end{bmatrix}, \tag{8}$$

where I_3 is a 3x3 identity matrix and 0_3 is a 3x3 matrix with all 0 entries.

The covariance $P_{k|k-1}$ associated to $\hat{\boldsymbol{x}}_{k|k-1}$ is also evaluated from the previous *a posteriori* $P_{k-1|k-1}$ and the process noise covariance matrix Q_k.

$$\boldsymbol{P}_{k|k-1} = F_k P_{k-1|k-1} F_k^T + Q_k, \tag{9}$$

$$Q_k = \begin{bmatrix} \Delta t_k^2 I_3/2 \\ \Delta t_k I_3 \\ I_3 \end{bmatrix} \begin{bmatrix} \sigma_{\breve{a}_1}^2 & 0 & 0 \\ 0 & \sigma_{\breve{a}_2}^2 & 0 \\ 0 & 0 & \sigma_{\breve{a}_3}^2 \end{bmatrix} \begin{bmatrix} \Delta t_k^2 I_3/2 \\ \Delta t_k I_3 \\ I_3 \end{bmatrix}^T, \tag{10}$$

where $\breve{a}_1^2, \breve{a}_2^2$ and $\breve{a}_3^2$ are the variances of an independent random accelerations that allow to track the different forces that could temporally affect target's dynamics (*e.g.*, friction) [1].

Update phase

This phase occurs at time k, when an observation vector $\boldsymbol{z}_k$ becomes available. This vector is modelled as follows [1]:

$$\begin{aligned} \boldsymbol{z}_k &= h(\boldsymbol{x}_k) + v_k, \\ \boldsymbol{v}_k &\sim \mathcal{N}(\boldsymbol{0}, R_k), \end{aligned} \tag{11}$$

where $\boldsymbol{z}_k$ is the measurements vector at time k, h is the observation function, which estimates the expected measurements at the state $\boldsymbol{x}_k$ and $\boldsymbol{v}_k$ is the random observation

noise vector assumed to be normally distributed with zero mean and covariance matrix R_k.

The observations are modelled on the basis of the classical position and distance models [1]. The UWB-ranging measurements represent the observation vector $\boldsymbol{z}$ defined as the distances between the UWB-based wearable device and L connected *anchor* nodes. Note that L can change along the time.

$$\boldsymbol{z} = \begin{bmatrix} \tilde{d}_{\mathrm{ref}_1} & \cdots & \tilde{d}_{\mathrm{ref}_L} \end{bmatrix}^T, \tag{12}$$

where a generic distance $\tilde{d}_{\mathrm{ref}_l}$, where $l \in [1, L]$, is the estimated UWB ranging measurement. The measured distance can be modeled as:

$$\tilde{d}_{\mathrm{ref}_l} = d_{\mathrm{ref}_l} + \eta, \tag{13}$$

where η is the observation error and d_{ref_l} is the true ranging measurement defined as:

$$d_{\mathrm{ref}_l} = \mathrm{dist}\left(\boldsymbol{p}, \boldsymbol{p}_{\mathrm{ref}_l}\right) = \sqrt{\sum_{i=1}^{3} \left(p_i - p_{i,\mathrm{ref}_l}\right)^2}. \tag{14}$$

Typically the observation errors are modelled as uncorrelated white Gaussian noises so the covariance matrix R_k depends on the variance of the measurements $\sigma^2_{d_{\mathrm{ref}_l}}$, $l \in [1, L]$:

$$R_k = \mathrm{diag}\begin{pmatrix} \sigma^2_{d_{\mathrm{ref}_1,k}} & \cdots & \sigma^2_{d_{\mathrm{ref}_L,k}} \end{pmatrix}. \tag{15}$$

Consequently, the observation function h is defined as the distances between the position component of the state vector and the reference nodes:

$$h\left(\boldsymbol{x}_k\right) = \begin{bmatrix} \mathrm{dist}\left(\boldsymbol{p}_k, \boldsymbol{p}_{\mathrm{ref}_1}\right) \\ \vdots \\ \mathrm{dist}\left(\boldsymbol{p}_k, \boldsymbol{p}_{\mathrm{ref}_L}\right) \end{bmatrix} \tag{16}$$

since $h\left(\boldsymbol{x}_k\right)$ is non-linear, the Jacobian matrix H needs to be computed around the *a priori* state $\boldsymbol{x}_{k|k-1}$:

$$H_k = [H_k^{\mathrm{aux}} | \mathbf{0}_{L,6}], \tag{17}$$

where H_k^{aux} is defined as:

$H_k^{\mathrm{aux}} =$

$$\begin{bmatrix} \frac{p_{1,k|k-1} - p_{1,\mathrm{ref}_1}}{\mathrm{dist}\left(\boldsymbol{p}_{k|k-1}, \boldsymbol{p}_{\mathrm{ref}_1}\right)} & \frac{p_{2,k|k-1} - p_{2,\mathrm{ref}_1}}{\mathrm{dist}\left(\boldsymbol{p}_{k|k-1}, \boldsymbol{p}_{\mathrm{ref}_1}\right)} & \frac{p_{3,k|k-1} - p_{3,\mathrm{ref}_1}}{\mathrm{dist}\left(\boldsymbol{p}_{k|k-1}, \boldsymbol{p}_{\mathrm{ref}_1}\right)} \\ \vdots & \vdots & \vdots \\ \frac{p_{1,k|k-1} - p_{1,\mathrm{ref}_L}}{\mathrm{dist}\left(\boldsymbol{p}_{k|k-1}, \boldsymbol{p}_{\mathrm{ref}_L}\right)} & \frac{p_{2,k|k-1} - p_{2,\mathrm{ref}_L}}{\mathrm{dist}\left(\boldsymbol{p}_{k|k-1}, \boldsymbol{p}_{\mathrm{ref}_L}\right)} & \frac{p_{3,k|k-1} - p_{3,\mathrm{ref}_L}}{\mathrm{dist}\left(\boldsymbol{p}_{k|k-1}, \boldsymbol{p}_{\mathrm{ref}_L}\right)} \end{bmatrix},$$

and $\mathbf{0}_{L,6}$ is a Lx6 matrix with all 0 entries.

The *a posteriori* state estimate $\hat{\boldsymbol{x}}_{k|k}$ and the corresponding covariance matrix $\hat{P}_{k|k}$ are estimated by correcting the *a priori* state estimate $\hat{\boldsymbol{x}}_{k|k-1}$ and the *a priori* state covariance matrix $\hat{P}_{k|k-1}$ with the following equations.

$$\hat{\boldsymbol{x}}_{k|k} = \hat{\boldsymbol{x}}_{k|k-1} + K_k \tilde{\boldsymbol{y}}_k, \tag{18}$$

$$P_{k|k} = \left(I_9 - K_k H_k\right) P_{k|k-1}, \tag{19}$$

where $\tilde{\boldsymbol{y}}_k$ is the innovation vector and K_k is the optimal Kalman gain defined as:

$$\tilde{\boldsymbol{y}}_k = \boldsymbol{z}_k - h\left(\hat{\boldsymbol{x}}_{k|k-1}\right), \tag{20}$$

$$K_k = P_{k|k-1} H_k^T S_k^{-1}, \tag{21}$$

where S_k is the covariance matrix computed as the expected measurement estimation error due to the *a priori* state error covariance plus the observation errors R_k.

$$S_k = H_k P_{k|k-1} H_k^T + R_k. \tag{22}$$

6. EXPERIMENTAL RESULTS

To evaluate the performance of the hybrid localization algorithm, an experimental campaign with dynamic conditions has been performed. Four UWB *anchor* nodes have been deployed in an indoor office area of 12 m × 9 m as depicted in Figure 4. The UWB-based wearable device (presented in section 4) has been used as *tag* worn by a person (named *the subject*), on the waist, at a height of 1.11 m performing ranging measurements with respect to all four *anchors* every 0.333 s. Accelerometer and gyroscope sensors have been sampled every 0.05 s while the magnetometer sensor every 0.1 s. The selected coordinates system is NED, which is the same used by the IMU/Magnetometer sensors.

During the experiment, the *subject* moved around the office in a moderate and steady way. In order to acquire the true position of the target along the time, the path followed by the *subject* has been marked with a metric tape attached to the floor. Besides, a laser has been used pointing down to the metric tape, which indicates the exact position of the UWB antenna. In addition, a camera has been used to register the laser point on the floor coinciding with the exact position of the *tag*. After that, the positions estimated by the algorithm have been compared with the exact ones taken, from the camera at the same time stamps, to calculate the accuracy. All raw data have been logged via USB on a PC and used to evaluate the performance off-line. Doing so, it has been possible to analyze our proposed algorithm and compare it with an UWB-only algorithm based on an EKF [1] using the PV model.

First of all, the logged raw data have been processed in order to set the correct parameters into the localization algorithms (*i.e.*, hybrid, PV EKF). For instance, the statistics for the ranging error were: average 0.37 m, standard deviation 0.21 m. Then the average value, which coincides with the bias, has been used to correct all range measurements. The settings for the UWB communication were: channel 2 (3993.6 MHz) at a bandwidth of 499.2 MHz and a data rate of 110 kbps. In order to use the ZA and SP detectors, presented in section 5.1, the magnitude of the accelerometer and gyroscope readings have been sampled in static conditions and then averaged providing 1.002 g and 0.0019 rad/sec, respectively. The error of the IMU measurements have been modeled according to the data sheet specifications.

Since the experiment has been carried out in an indoor environment, magnetic disturbances might be expected, thus affecting the performance of the *Attitude estimator*. It is clear then, that the performance of the hybrid localization strongly depends on the *Attitude estimator* efficiency.

Figure 4 shows the positions estimated by the proposed hybrid algorithm (described in section 5) and the UWB-only approach using the PV EKF [1]. In addition, the figure shows the true path and the locations of the *anchors*. Since the experiment has been performed at a constant height, the final location error has been analysed in 2D. The localization frequency has been set to 3 Hz for both algorithms (corresponding to the ranging measurement frequency). Localization at higher frequencies is not of interest for this experiment since the application is focused on pedestrian localization. It is worth mentioning that the hybrid algorithm would also be able to track the position at two higher frequencies, 10 Hz and 20 Hz corresponding to the sample frequency of the magnetometer and gyroscope, respectively.

The calculated RMS of the localization error is 0.23 m for

the hybrid algorithm and 0.4 m for the PV EKF algorithm, while the availability is 100% and 63.7%, respectively. The position availability for the PV EKF depends directly on the number of collected ranging measurements from *anchors*. Instead, for the hybrid algorithm there are no constraints regarding the *anchor* connectivity. As mentioned in section 5.2, the *Location estimator* can provide an estimated position in two moments; during the *predict phase* in absence of ranging, and *update phase* when ranging is available. However, the position provided by the *predict phase* can be used only for a short period of time because the bias correction for the accelerometer, which is part of the *update phase*, is not executed. Thus, apart from the accuracy, another advantage of the hybrid algorithm is the increased availability in harsh environments. This advantage could be exploited to reduce the number of *anchors* while meeting a desired level of performance. Additionally, the registered average ranging availability with four *anchors* was 74.1%. Note that a ranging measurement is considered available when both *tag* and *anchor* are able to exchange messages. The maximum range strongly depends on the environment. Typically, it is approximately 249 m in LoS and 27 m in NLoS.

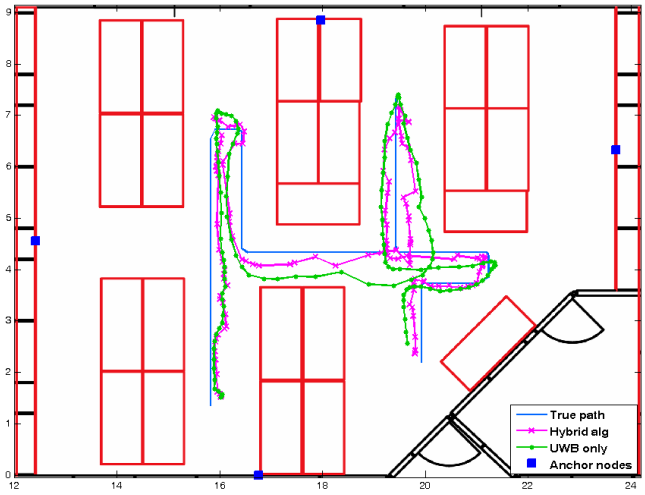

Figure 4: Plot of the location estimation.

7. CONCLUSION

This paper proposed a hybrid localization algorithm, combining UWB-based ranging measurements and IMU data, able to work in harsh industrial environments for pedestrian localization. This work has been motivated by the occupational safety scenario that is of great interest in the era of Industry 4.0. In order to improve the localization performance, the proposed hybrid algorithm has been based on the adoption of several existing filter techniques and disturbance measurement detectors that provide a reliable asset estimation. The estimation of the orientation is an input to the proposed hybrid PVA EKF block. The hybrid algorithm has been further improved by integrating a filter that removes ranging measurements outliers. To evaluate the localization performance in an indoor environment, the designed hybrid algorithm has been implemented in a proprietary wearable platform. This wearable device has also allowed the storage of the raw data into a PC for further off-line analysis.

The PV EKF algorithm [1], which is based only on UWB raging measurements, has been chosen as benchmark. Taking as input the collected experimental data, the proposed hybrid algorithm has provided a localization RMS error of 0.23 m and availability of 100%, outperforming the PV EKF algorithm, which has shows a localization error of 0.45 m and availability of 63.7%.

The main advantages of the proposed algorithm with respect to the PV EKF were: improved location accuracy, improved availability, accurate *attitude* estimation and the possibility to use higher localization update rates. The improved location availability could be used to reduce the number of *anchors* required while meeting a required level of performance; thus saving deployment costs and hardware maintenance. In addition, the modular approach adopted in the hybrid algorithm implementation led to a reduction of computational processing in comparison with other hybrid implementations [4]. In fact, the processing cost is saved because the matrixes are smaller.

8. ACKNOWLEDGMENTS

This work was partially supported by the European H2020 project SatisFactory, under contract no: 636302.

9. REFERENCES

[1] M. A. Caceres, F. Sottile, and M. A. Spirito. Adaptive location tracking by kalman filter in wireless sensor networks. In *2009 IEEE International Conference on Wireless and Mobile Computing, Networking and Communications*, pages 123–128, Oct 2009.

[2] E. M. Diaz, F. de Ponte Müller, A. R. Jiménez, and F. Zampella. Evaluation of ahrs algorithms for inertial personal localization in industrial environments. In *2015 IEEE International Conference on Industrial Technology (ICIT)*, pages 3412–3417, March 2015.

[3] E. M. Diaz, A. L. M. Gonzalez, and F. de Ponte Müller. Standalone inertial pocket navigation system. In *2014 IEEE/ION Position, Location and Navigation Symposium - PLANS 2014*, pages 241–251, May 2014.

[4] T. Gaedeke, M. Johnson, M. Hedley, and W. Stork. Fusion of wireless ranging and inertial sensors for precise and scalable indoor localization. In *2014 IEEE International Conference on Communications Workshops (ICC)*, pages 138–143, June 2014.

[5] S. Gezici, Z. Tian, G. B. Biannakis, H. Kobayashi, A. F. Molisch, V. Poor, Z. Sahinoglu, S. Gezici, Z. Tian, G. B. Giannakis, H. Kobayashi, A. F. Molisch, H. V. Poor, and Z. Sahinoglu. Localization via ultra-wideband radios. In *IEEE Signal Processing Magazine*, pages 70–84, 2005.

[6] F. Hartmann, T. Gaedeke, P. Leibold, L. Niestoruk, and W. Stork. Navigation for occupational safety in harsh industrial environments. In *Smart Objects, Systems and Technologies (Smart SysTech), 2014 European Conference on*, pages 1–8, July 2014.

[7] IEEE. IEEE 802.15.4-2015 - IEEE Standard for Low-Rate Wireless Networks. 2015.

[8] A. R. Jiménez, F. Seco, J. C. Prieto, and J. Guevara. Indoor pedestrian navigation using an ins/ekf framework for yaw drift reduction and a foot-mounted imu. In *Positioning Navigation and Communication*

(WPNC), 2010 7th Workshop on, pages 135–143, March 2010.

[9] A. Lewandowski and C. Wietfeld. A comprehensive approach for optimizing toa-localization in harsh industrial environments. In *Position Location and Navigation Symposium (PLANS), 2010 IEEE/ION*, pages 516–525, May 2010.

[10] W. Li and J. Wang. Effective adaptive kalman filter for mems-imu/magnetometers integrated attitude and heading reference systems. *Journal of Navigation*, 66(1):99–113, 007 2012.

[11] D. Lucke, E. Westkamper, M. Eissele, T. Ertl, and O. Siemoneit. Privacy-preserving self-localization techniques in next generation manufacturing an interdisciplinary view on the vision and implementation of smart factories. In *Control, Automation, Robotics and Vision, 2008. ICARCV 2008. 10th International Conference on*, pages 1183–1188, Dec 2008.

[12] K. Zhou, T. Liu, and L. Zhou. Industry 4.0: Towards future industrial opportunities and challenges. In *Fuzzy Systems and Knowledge Discovery (FSKD), 2015 12th International Conference on*, pages 2147–2152, Aug 2015.